# Fullerene-Based Supramolecular Nanoclusters with poly[2-methoxy-5-(2'-ethylhexyloxy)-*p*-phenylenevinylene] (MEH-PPV) for Light Energy Conversion

Taku Hasobe,[*,a,b] Shunichi Fukuzumi,[c] Prashant V. Kamat,[d] and Hideyuki Murata[a]

[a]School of Materials Science, Japan Advanced Institute of Science and Technology (JAIST), 1-1, Asahidai, Nomi, Ishikawa, 923-1292, Japan

[b]Research Center for Integrated Science, JAIST, Nomi, Ishikawa, 923-1292, Japan

[c]Department of Material and Life Science, Division of Advanced Science and Biotechnology, Graduate School of Engineering, Osaka University, SORST, Japan Science and Technology Agency (JST), Suita, Osaka 565-0871, Japan

[d]Notre Dame Radiation Laboratory and Departments of Chemistry & Biochemistry and Chemical & Biomolecular Engineering, University of Notre Dame. Notre Dame Indiana 46556-5674, USA

**KEYWORDS:** fullerene, MEH-PPV, porphyrin, organic solar cell, supramolecular assembly

E-mail Address: t-hasobe@jaist.ac.jp

**Abstract:** Organized composite molecular nanoassemblies of fullerene and poly[2-methoxy-5-(2'-ethylhexyloxy)-*p*-phenylenevinylene] (MEH-PPV) prepared in acetonitrile/toluene mixed solvent absorb light over entire spectrum of visible light. The highly colored composite clusters can be assembled as 3 dimensional array onto nanostructured $SnO_2$ films using electrophoretic deposition approach. The composite cluster films exhibit an incident photon-to-photocurrent efficiency (IPCE) as high as 18%, which is significantly higher than that of molecular assembly composed of 5,10,15,20-tetrakis(3,5-di-*tert*-butylphenyl)-21*H*,23*H*-porphyrin ($H_2P$) and $C_{60}$ prepared by the same manner (4%). The maximum IPCE value is increased to 25% under an applied bias potential to 0.2 V vs. SCE. The power conversion efficiency of MEH-PPV and $C_{60}$ assembly-modified electrode is determined as 0.24%. The photocurrent generation properties observed with MEH-PPV and $C_{60}$ clusters demonstrate the synergy of these systems towards yielding efficient photoinduced charge separation within these composite nanoclusters.

**Introduction**

The need to develop next generation solar cells has stimulated renewed interest in the design of efficient, low-cost energy conversion devices.[1-12] A promising and attractive strategy is to mimic natural photosynthesis. Energy from sunlight is captured by photosynthetic $\pi$-pigments (primarily chlorophylls and carotenoids) which cover the wide spectral range of the solar irradiation.[13,14] Light energy is absorbed by the individual $\pi$-pigments and is quickly transferred to chlorophylls that are in a well-organized protein environment. The energy conversion event start via electron-transfer processes. The artificial photoconversion devices developed so far have a limited degree of self-organization, whereas the components in the natural photosynthetic system are highly organized in quaternary protein structures. Although exact duplication of natural photosynthetic environment is not necessary for construction of artificial light energy conversion devices, little attention has been given to artificial light energy conversion devices based on highly organized light harvesting assemblies. The construction of efficient solar cells also requires an enhanced light-harvesting efficiency of chromophore molecules throughout the solar spectrum together with a highly efficient conversion of the harvested light into electrical energy. Thus, useful combination and organization of organic molecules is essential for light energy conversion properties.

Recently, progress is being made towards the development of bulk heterojunction organic solar cells, which possess an active layer of a conjugated donor polymer and an acceptor molecule.[2-5,7,8,10-12,15] In these blend systems, efficient photoinduced electron transfer occurs at the donor-acceptor interface, and intimate mixing of donor and acceptor is therefore beneficial for efficient charge separation. Especially, fullerene is used as a suitable electron acceptor component in such photovoltaic cells. The electron-transfer reduction of $C_{60}$ is highly efficient because of the minimal changes of structure and solvation associated with the electron-transfer reduction.[16-20] On the other hand, the conjugated polymer such as poly[2-methoxy-5-(2'-ethylhexyloxy) -*p*-phenylenevinylene]

(MEH-PPV) has also emerged as a promising photonic and donor polymer. Photonic devices incorporating MEH-PPV have thus far included light-emitting diodes[21,22] and photodiodes.[23] MEH-PPV-$C_{60}$ based photodetectors with high visible-ultraviolet sensitivity[24] and photovoltaic devices have also been fabricated.[25,26]

Porphyrins with its electron donating as well as sensitizing properties are suitable for efficient electron transfer with small reorganization energies.[18-20] In addition, rich and extensive absorption features of porphyrinoid systems guarantees increased absorption cross-sections and an efficient use of the solar spectrum.[27] Moreover, porphyrins and fullerenes are known to form supramolecular complexes facilitating close contact between one of the electron-rich 6:6 bonds of the guest fullerene and the geometric center of the host porphyrin.[28-33] The porphyrin-fullerene interaction energies are reported to be in the range of -16 to -18 kcal $mol^{-1}$.[34] Such a strong interaction between porphyrins and fullerenes is likely to be a good driving force for the formation of supramolecular complexes between porphyrin and $C_{60}$. Based on these ideas, we have recently developed highly organized supramolecular photovoltaic cells composed of fullerenes and multi-porphyrin arrays.[35,36] Although construction of molecular devices using a variety of molecular assemblies has already been attempted, new organization strategies and approaches for efficient light energy conversion are continuously sought to tailor their performance.

Herein we report new types of light energy conversion systems using fullerene-based supramolecular composites with an electron donor: MEH-PPV (Fig. 1), which are clusterized on nanostructured $SnO_2$ electrodes. The organized molecular assembly between fullerene and MEH-PPV prepared in acetonitrile/toluene mixed solution exhibit efficient light-harvesting and light energy conversion properties in the visible region. In addition, we have compared the structural and light energy conversion properties of fullerene and MEH-PPV–based assembly films with that of fullerene and 5,10,15,20-tetrakis(3,5-di-*tert*-butylphenyl)-21*H*,23*H*-porphyrin ($H_2P$) composite films. The details

on the dependence of photoelectrochemical properties on the different molecular organizations between donor and acceptor moieties are discussed.

**Fig. 1**

## 2. Experimental Section

### *2.1 General*

Melting points were recorded on a Yanagimoto micro-melting point apparatus and not corrected. $^{1}$H NMR spectra were measured on a JEOL EX-270 (270 MHz) or a JEOL JMN-AL300 (300 MHz). Matrix-assisted laser desorption/ionization (MALDI) time-of-flight mass spectra (TOF) were measured on a Kratos Compact MALDI I (Shimadzu). The UV-visible spectra were recorded on a Perkin Elmer LAMDA 750 spectrophotometer. Transmission electron micrographs (TEM) of porphyrin and fullerene assemblies were recorded by applying a drop of the sample to carbon-coated copper grid. Images were recorded using a Hitachi H7100 transmission electron microscope.

### *2.2 Materials*

All solvents and chemicals were of reagent grade quality, obtained commercially and used without further purification unless otherwise noted (*vide infra*). Thin-layer chromatography (TLC) and flash column chromatography were performed with Art. 5554 DC-Alufolien Kieselgel 60 $F_{254}$ (Merck), and Fujisilicia BW300, respectively. Nanostructured $SnO_2$ films were cast on an optically transparent electrode (OTE) by applying a 2% colloidal solution obtained from Alfa Chemicals. The air-dried films were annealed at 673 K. The details of the preparation of $SnO_2$ films on conducting glass substrate were reported elsewhere.[37)] The nanostructured $SnO_2$ film electrode is referred as OTE/$SnO_2$. Poly[2-methoxy-5-(2-ethylhexyloxy)-1,4-phenylenevinylene]

(MEH-PPV) were purchased from Aldrich ($M_n$:~51,000). Preparation of $H_2P$ have been described elsewhere.[35)]

*2.3 Electrophoretic Deposition of Molecular Cluster Films*

A known amount of MEH-PPV, porphyrin, and $C_{60}$ or mixed cluster solution in acetonitrile/toluene (3/1, v/v, 2 mL) was transferred to a 1 cm cuvette in which two electrodes (viz., OTE/$SnO_2$ and OTE) were kept at a distance of 6 mm using a Teflon spacer. A dc electric field (~200V/cm) was applied between these two electrodes using a Fluke 415 power supply. The deposition of the film can be visibly seen as the solution becomes colorless with simultaneous brown coloration of the OTE/$SnO_2$ electrode. The OTE/$SnO_2$ electrode coated with MEH-PPV and $C_{60}$ clusters is referred as OTE/$SnO_2$/(MEH-PPV+$C_{60}$)$_n$. Preparation of ($H_2P$+$C_{60}$)$_n$ is also adopted by the same method as $H_2P$-$C_{60}$ composites ([$H_2P$] = 0.19 mM and [$C_{60}$] = 0.31 mM in acetonitrile/toluene = 3/1, v/v). The weight % ratio of MEH-PPV : $C_{60}$ is ~ 1 : 4. The final concentration of $C_{60}$ is 0.31 mM.

*2.4 Photoelectrochemical Measurements*

Photoelectrochemical measurements were carried out using a working electrode and a Pt gauge counter electrode in the cell assembly using a Keithley model 617 programmable electrometer. The electrolyte was 0.5 M NaI and 0.01 M $I_2$ in acetonitrile. A collimated light beam from a 150 W Xenon lamp with a 400 nm cut-off filter was used for excitation of (MEH-PPV+$C_{60}$)$_m$ films deposited on $SnO_2$ electrodes. A Bausch and Lomb high intensity grating monochromator was introduced into the path of the excitation beam for the selected wavelength.

The incident photon to photocurrent efficiency (IPCE) values were calculated by normalizing the photocurrent values to incident light energy and intensity using eq 1,[38)]

$$\text{IPCE}\ (\%) = 100 \times 1240 \times I_{sc}/(I_{inc} \times \lambda) \quad (1)$$

where $I_{sc}$ is the short circuit photocurrent (A/cm$^2$), $I_{inc}$ is the incident light intensity (W/cm$^2$), and $\lambda$ is the wavelength (nm).

Power conversion efficiency, $\eta$ is calculated by eq 2,[38]

$$\eta = FF \text{ x } I_{sc} \text{ x } V_{oc}/W_{in} \quad (2)$$

where the fill factor (*FF*) is defined as $FF = [IV]_{max}/ I_{sc} V_{oc}$, where $V_{oc}$ is the open circuit photovoltage, and $I_{sc}$ is the short circuit photocurrent.

## 3. Result and Discussion

### *3.1 Construction of Molecular Assemblies of Fullerenes and Donor moieties*

$C_{60}$, MEH-PPV and porphyrin are soluble in nonpolar solvents such as toluene, but sparingly soluble in polar solvents such as acetonitrile.[38,39] When a concentrated solution of these molecules in toluene is mixed with acetonitrile by fast injection method, the molecules aggregate and form stable clusters. The final solvent ratio of mixed solvent employed in the present experiments was 3 : 1 (v/v) acetonitrile : toluene. The same strategy can be extended to prepare mixed or composite molecular clusters consisting of donor moieties and $C_{60}$ molecules. Mixed cluster aggregates in the present investigation were prepared by mixed solution containing constant molar ratio of donor moieties (MEH-PPV or $H_2P$) and $C_{60}$ in toluene (0.5 ml), and then injecting into a pool of acetonitrile (1.5 ml). These optically transparent composite clusters [denoted as (MEH-PPV+$C_{60}$)$_n$ and ($H_2P$+$C_{60}$)$_n$] are stable at room temperature and they can be reverted back to their monomeric forms by diluting the solution with toluene.

The absorption spectra of donor moieties (MEH-PPV and $H_2P$) and $C_{60}$ in neat

toluene are compared with the absorption spectrum of [(MEH-PPV+$C_{60}$)$_n$ or ($H_2$P+$C_{60}$)$_n$] clusters in acetonitrile/toluene (3/1, v/v) in Fig. 2. In both cases, the composite clusters [(MEH-PPV+$C_{60}$)$_n$ or ($H_2$P+$C_{60}$)$_n$] in the mixed solvent (spectra a) exhibit much broader and more intense absorption in the visible and near infrared regions than those of parent MEH-PPV (or $H_2$P) in spectra b and $C_{60}$ in spectra c. For example, earlier studies on the porphyrin clusters have shown that the intermolecular interactions have significant impact on the intensity and position of the Soret and Q-bands.[40] In the case of ($H_2$P+$C_{60}$)$_n$, although Soret band of unaggregated monomeric $H_2$P remains, Q-bands become red-shifted. The presence of $C_{60}$ induces further enhancement of absorption of these clusters in the visible region. This demonstrates that the composite clusters of donor moieties and $C_{60}$ are superior light absorbers as compared to that of the corresponding single component since they absorb throughout the visible part of the solar spectrum. A charge transfer type interaction between the two molecules may be responsible for the long-wavelength absorption of the composite clusters. Similar charge transfer interactions leading to extended absorption has been observed for donor-$C_{60}$ composites[41-43] linked at close proximity.

**Fig. 2**

Fig. 3 shows transmission electron micrographs (TEM) images of (MEH-PPV+$C_{60}$)$_n$ and ($H_2$P+$C_{60}$)$_n$ to examine the structural properties of these molecular assemblies. The TEM image of (MEH-PPV+$C_{60}$)$_n$ (Fig. 3A) displays well-controlled size and shape of nanoclusters with a diameter of ~50 nm. These clusters are in sharp contrast with the TEM image of ($H_2$P+$C_{60}$)$_n$ exhibiting irregular and larger size (Fig. 3B). Judging from the molecular scales of these molecules, one can safely conclude that MEH-PPV is self-assembled with $C_{60}$ molecules in the mixed solution to yield large donor–acceptor (D-A) nanoclusters with an interpenetrating network.

**Fig. 3**

*3.2 Solar Energy Conversion Properties of (MEH-PPV+$C_{60}$)$_n$ and ($H_2P$+$C_{60}$)$_n$ Assemblies-Modified Electrode using Two-electrode System*

As shown earlier,[44,45] clusters of $C_{60}$ prepared in acetonitrile/toluene mixed solvent can be assembled electrophoretically as thin films on a conducting glass electrode surface. A similar electrodeposition approach was adopted to prepare film of (MEH-PPV+$C_{60}$)$_n$ or ($H_2P$+$C_{60}$)$_n$ on nanostructured $SnO_2$ films cast on an optically conducting glass electrode (referred as OTE/$SnO_2$). Upon application of the DC electric field of ~200 V/cm between OTE/$SnO_2$ and OTE electrodes which were immersed parallel in a mixed acetonitrile/toluene (3/1, v/v) solution containing (MEH-PPV+$C_{60}$)$_n$ or ($H_2P$+$C_{60}$)$_n$ clusters we can achieve deposition of mixed clusters on $SnO_2$ nanocrystallites. As the deposition continues we can visually observe discoloration of the solution and coloration of the electrode that is connected to positive terminal of the dc power supply. Fig. 4 shows an absorption spectrum of OTE/$SnO_2$/(MEH-PPV+$C_{60}$)$_n$ film prepared by electrophoretic deposition. The absorption spectrum exhibits a broad photoresponse, which is consistent with the absorption spectrum of aggregated molecular clusters in acetonitrile/toluene (spectrum a in Fig. 2A).[46] The ability to assemble clusters from solution onto electrode surface demonstrates that electrophoretic deposition is useful for fabrication of organic thin films.

**Fig. 4**

In order to evaluate the photoelectrochemical performance of the (MEH-PPV+$C_{60}$)$_n$, we used the OTE/$SnO_2$/(MEH-PPV+$C_{60}$)$_n$ electrode as a photoanode in a photoelectrochemical cell. Photocurrent measurements were performed in acetonitrile

containing NaI (0.5 M) and $I_2$ (0.01 M) as redox electrolyte using a Pt gauge counter electrode (Fig. 5).[38] We also constructed an OTE/$SnO_2$/$(H_2P+C_{60})_n$ electrode to compare the light energy conversion properties in the presence and absence of MEH-PPV (Fig. 5). The photocurrent and photovoltage responses recorded following the excitation of OTE/$SnO_2$/$(MEH\text{-}PPV+C_{60})_n$ electrode are shown in Fig. 6A and B, respectively. The photocurrent response is prompt, steady and reproducible during repeated on/off cycles of the visible light illumination. The short circuit photocurrent density ($i_{sc}$) is 0.31 mA/cm$^2$, and open circuit voltage ($V_{oc}$) is 220 mV were reproducibly obtained during these measurements. Blank experiments conducted with OTE/$SnO_2$ [i.e., by excluding composite clusters: $(MEH\text{-}PPV+C_{60})_n$] produced no detectable photocurrent under the similar experimental conditions. These experiments confirmed the role of $(MEH\text{-}PPV+C_{60})_n$ assemblies towards harvesting light energy and generating photocurrent during the operation of a photoelectrochemical cell.

**Fig. 5 and Fig. 6**

We also evaluated the power characteristics of the photoelectrochemical cell by varying the load resistance. A drop in the photovoltage and an increase in the photocurrent are observed with decreasing the load resistance (Fig. 7). The fill factor for the $(MEH\text{-}PPV+C_{60})_n$-based photoelectrochemical cell was determined to be 0.40. Net power conversion efficiency obtained for the same cell was 0.24% (input power: 11.2 mW/cm$^2$). This value is ~7 times larger than 0.035% of OTE/$SnO_2$/$(H_2P+C_{60})_n$ (trace b).

**Fig. 7**

In order to further evaluate the response of $(MEH\text{-}PPV+C_{60})_n$ clusters towards the photocurrent generation a series of photocurrent action spectra were recorded and

compared against the $(H_2P+C_{60})_n$ clusters. The photocurrent action spectrum of OTE/$SnO_2$/$(MEH\text{-}PPV+C_{60})_n$ produced by the electrodeposition of MEH-PPV and $C_{60}$ is shown in spectrum a of Fig. 8. The photocurrent action spectrum exhibits a broad photoresponse, which approximately parallel the corresponding absorption spectrum.[47] The maximum IPCE value of OTE/$SnO_2$/$(MEH\text{-}PPV+C_{60})_n$ attains 18% at 480 nm, which is ~5 times larger than 4% of OTE/$SnO_2$/$(H_2P+C_{60})_n$. Both the *I-V* characteristic (trace b in Fig. 7) and the intensity dependence of the efficiency (spectrum b in Fig. 8) in OTE/$SnO_2$/$(H_2P+C_{60})_n$ show that charge recombination and charge transport within the nanostructure assembly is a major limiting factor in achieving higher photoconversion efficiencies. However, we have recently reported that composite clusters of multi-porphyrin arrays such as porphyrin alkanethiolate monolayer-protected gold nanoparticles and fullerenes ($C_{60}$), which were assembled on a nanostructured $SnO_2$ electrode using a similar deposition technique, exhibited much enhanced light energy conversion properties ($\eta$: ~1.5%) as compared with the non-organized systems (0.035%).[35,36] This drastic enhancement (~45 times) of the power conversion efficiency is largely ascribed to the organization between donor and acceptor moieties on the OTE/$SnO_2$ electrode for the efficient initial photoinduced electron transfer.

**Fig. 8**

*3.3 Photoelectrochemical Properties of $(MEH\text{-}PPV+C_{60})_n$ and $(H_2P+C_{60})_n$ Assemblies-Modified Electrode using Three-Electrode System*

The charge separation in the OTE/$SnO_2$/$(MEH\text{-}PPV+C_{60})_n$ electrode assembly can be further modulated by using them in a standard three-compartment cell as a working electrode along with Pt wire gauze counter electrode and saturated calomel reference electrode (SCE).[48] Figure 9A shows *I-V* characteristics of the OTE/$SnO_2$/$(MEH\text{-}PPV+C_{60})_n$ electrode under the visible light illumination. The photocurrent increases as

the applied potential is scanned towards more positive potentials. Increased charge separation and the facile transport of charge carriers under positive bias are responsible for enhanced photocurrent generation. At potentials greater than +0.4 V *vs*. SCE direct electrochemical oxidation of iodide interferes with the photocurrent measurement. Since we can control the photocurrent generation property by applying bias to OTE/$SnO_2$, we have also optimized a photocurrent action spectrum of OTE/$SnO_2$/(MEH-PPV+$C_{60}$)$_n$ under an applied bias potential of 0.2 V vs. SCE (spectrum a in Fig. 9B). The action spectrum also shows a broad photoresponse and a maximum IPCE value of 25%. This value is larger than the value measured in two electrode system (18%: spectrum b).

### *3.4 Photocurrent Generation Mechanism*

The photoinduced charge separation processes in MEH-PPV-$C_{60}$ and $H_2P$-$C_{60}$ are already established.[35,49,50] The primary process responsible for the photocurrent generation is the photoinduced charge separation between the excited state of MEH-PPV or $H_2P$[38] to $C_{60}$ ($C_{60}/C_{60}^{\bullet-}$ = -0.2 V vs NHE) in the donor mieties-$C_{60}$ supramolecular complex. This electron transfer process within the aggregated cluster is fast compared to the direct electron injection to the conduction band of $SnO_2$ (0 V vs NHE) system. As the reduced $C_{60}$ injects electrons into the $SnO_2$ nanocrystallites, the oxidized MEH-PPV (MEH-PPV/MEH-PPV$^{\bullet+}$ = 1.0 vs NHE)[51] or $H_2P$ ($H_2P/H_2P^{\bullet+}$ = 1.2 V vs NHE) undergoes electron transfer with iodide ion ($I_3^-/I^-$ = 0.5 V vs NHE) in the electrolyte.[38] Such a photocurrent generation mechanism is consistent with the earlier reported reaction scheme involving organized donor-acceptor assemblies.[35,36,48]

## 4. Conclusions

The supramolecular assemblies of fullerene-based composites composed of MEH-PPV provide useful systems for fulfilling an enhanced light-harvesting efficiency of chromophores throughout the solar spectrum and a highly efficient conversion of the harvested light into the high energy state of the charge separation by photoinduced electron transfer. Especially, the structure of $(\text{MEH-PPV}+C_{60})_n$ has well-controlled size and shape as compared to that of $(H_2P+C_{60})_n$. The photoelectrochemical behavior of $\text{OTE}/SnO_2/(\text{MEH-PPV}+C_{60})_n$ also exhibits much enhancement as compared to those of $(H_2P+C_{60})_n$. Such systems based on supramolecular approach have promising perspective for the development of efficient light energy conversion devices.

**Acknowledgment**

This work was partially supported by Grant–in–Aids for Scientific Research (No. 19710119 to T.H.) and special coordination funds for promoting science and technology from the Ministry of Education, Culture, Sports, Science and Technology, Japan. T.H. also acknowledges the partial support from Kao Foundation for Arts and Sciences, Iketani Science and Technology Foundation, and Kansai Research Foundation for Technology Promotion. P.V.K. acknowledges the support from the Office of Basic Energy Science of the U.S. Department of Energy. This is contribution no. NDRL 4734 from the Notre Dame Radiation Laboratory.

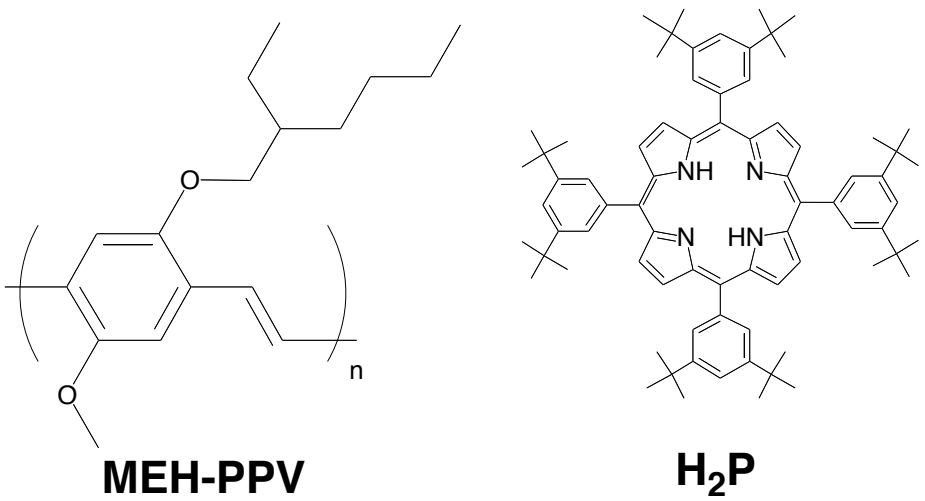


**Fig. 1** Molecular structures of MEH-PPV and $H_2P$ used in this study.

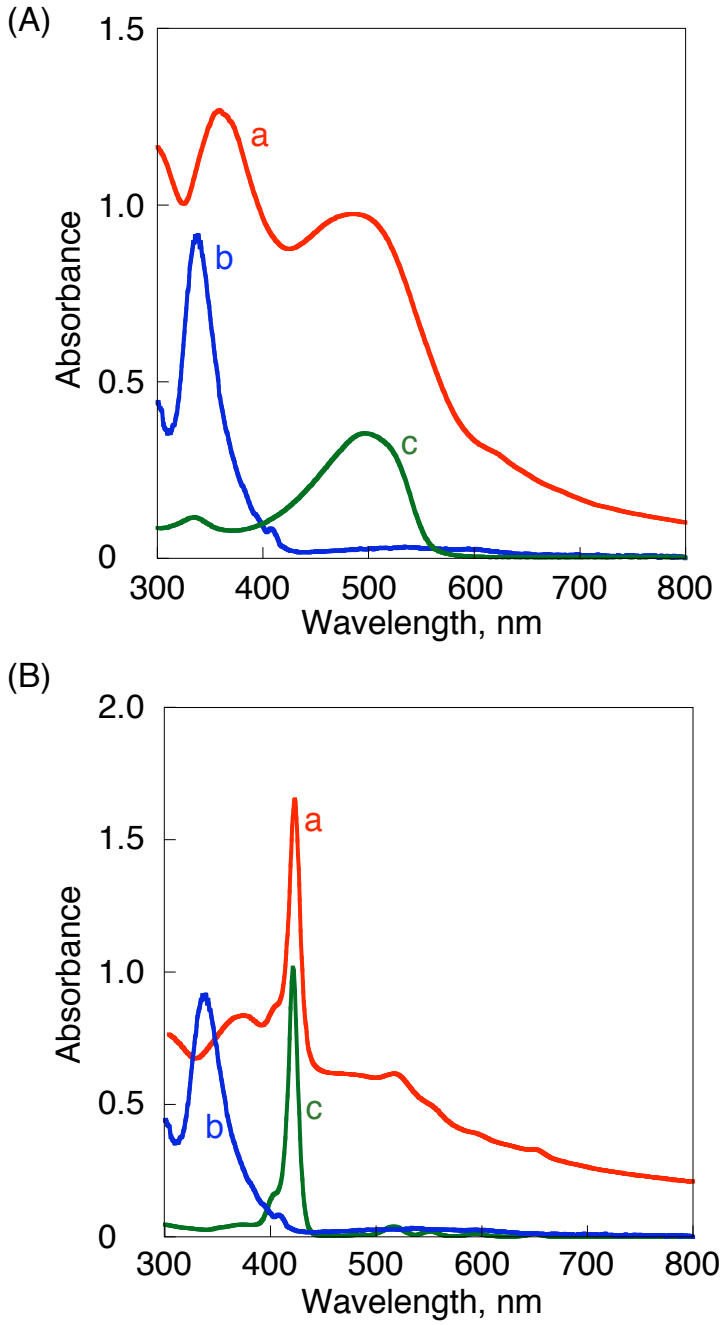


**Fig. 2** (A) Absorption spectra of (a) $(MEH\text{-}PPV+C_{60})_n$ in acetonitrile/toluene (3/1, v/v). The weight % ratio of MEH-PPV : $C_{60}$ is ~ 1 : 4; $[C_{60}]$ = 0.31 mM. (b) $C_{60}$ (75 µM) in toluene and (c) MEH-PPV in toluene. (B) Absorption spectra of (a) $(H_2P+C_{60})_n$ in acetonitrile/toluene (3/1, v/v); $[H_2P]$ = 0.19 mM and $[C_{60}]$ = 0.31 mM, (b) $C_{60}$ (75 µM) in toluene and (c) $H_2P$ (11 µM) in toluene.

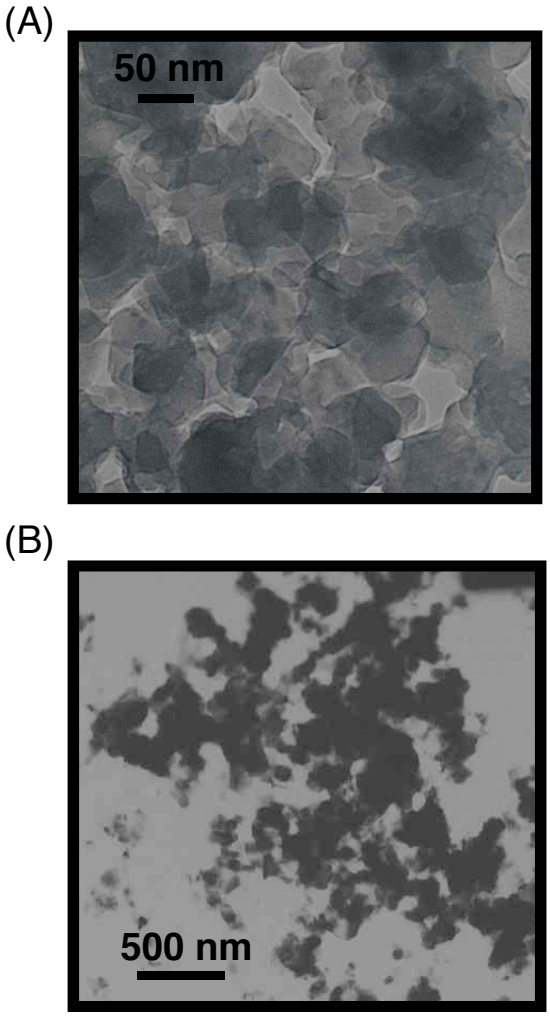


**Fig. 3** Transmission electron micrograph (TEM) images of (A) $(MEH\text{-}PPV+C_{60})_n$ and (B) $(H_2P+C_{60})_n$.

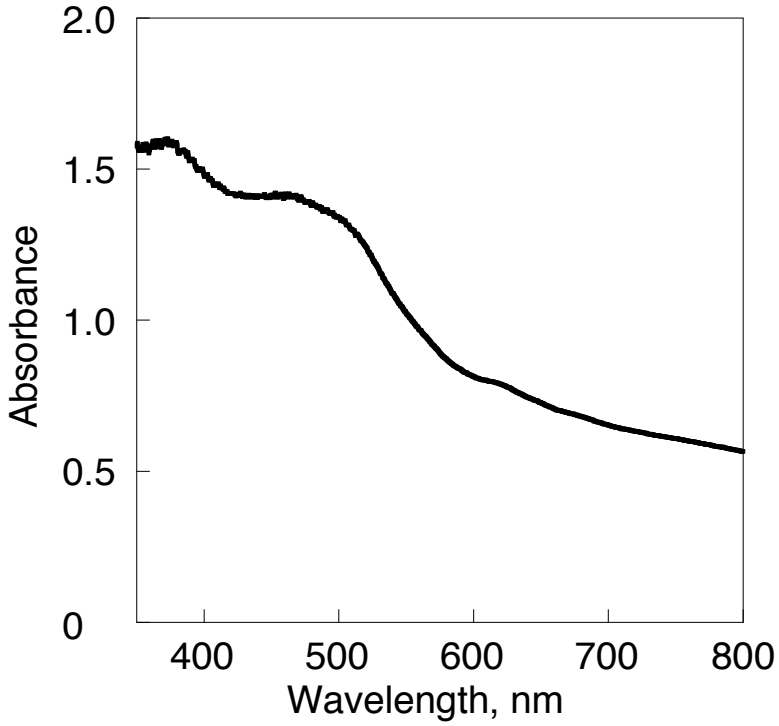


**Fig. 4** Absorption spectrum of OTE/$SnO_2$/(MEH-PPV+$C_{60}$)$_n$ film.

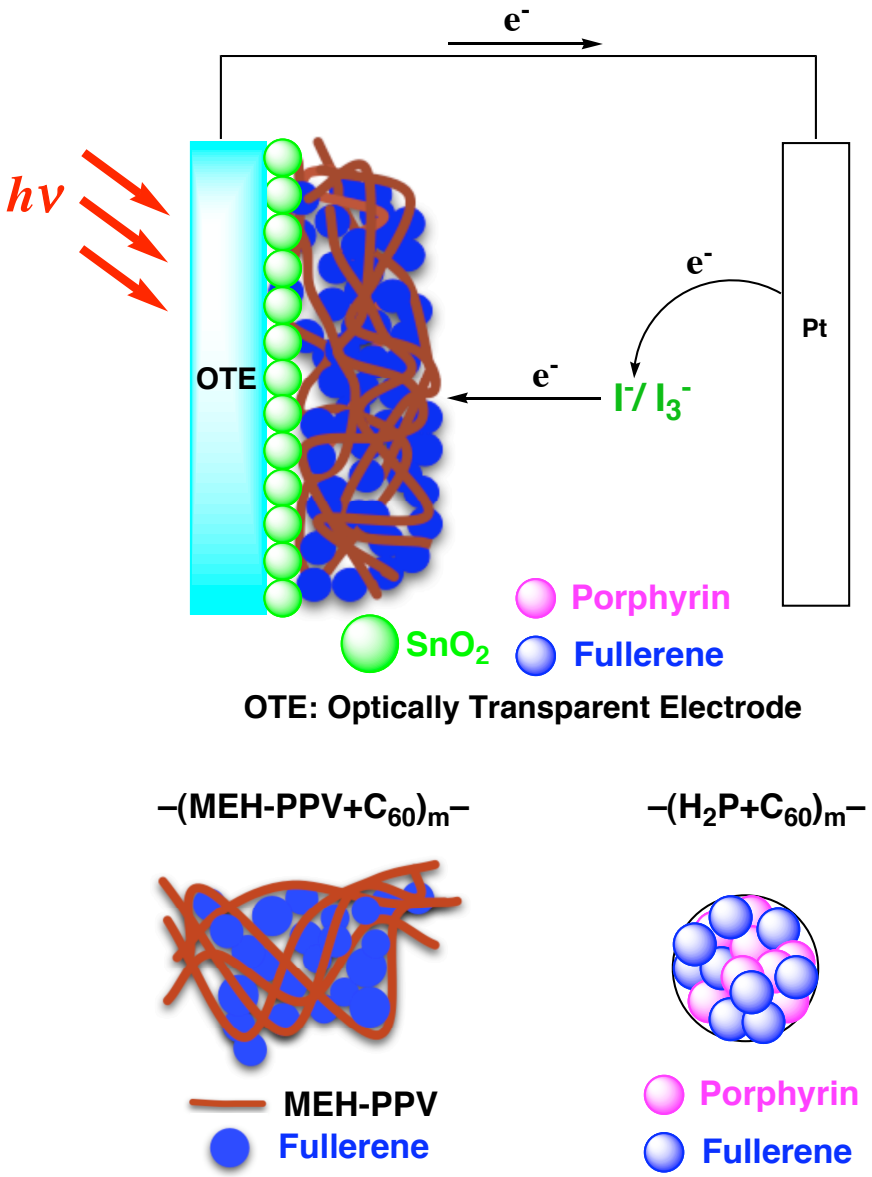


**Fig. 5** Operation of a photochemical solar cell using molecular assembly of MEH-PPV and $C_{60}$ [$(MEH\text{-}PPV+C_{60})_n$], and schematic illustrations of $(MEH\text{-}PPV+C_{60})_n$ and $(H_2P+C_{60})_n$ as the photoactive layers.

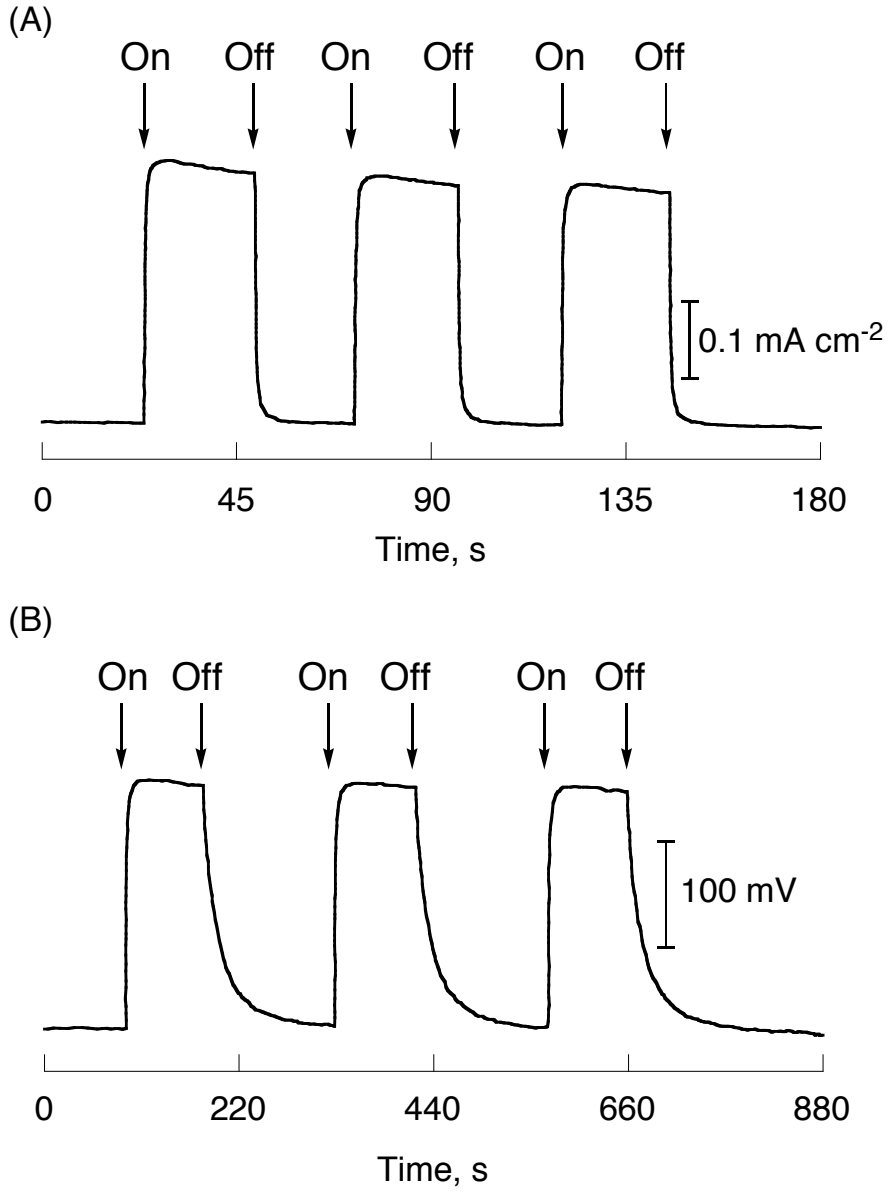


**Fig. 6** (A) Photocurrent response and (B) photovoltage response of OTE/$SnO_2$/(MEH-PPV+$C_{60}$)$_n$ electrode prepared from cluster solution of ([$C_{60}$] = 0.31 mM: weight % ratio of MEH-PPV : $C_{60}$ is ~ 1 : 4 ) to visible light illumination ($\lambda > 400$ nm); electrolyte: 0.5 M NaI and 0.01M $I_2$ in acetonitrile; Input Power: 11.2 mW cm$^{-2}$.

.

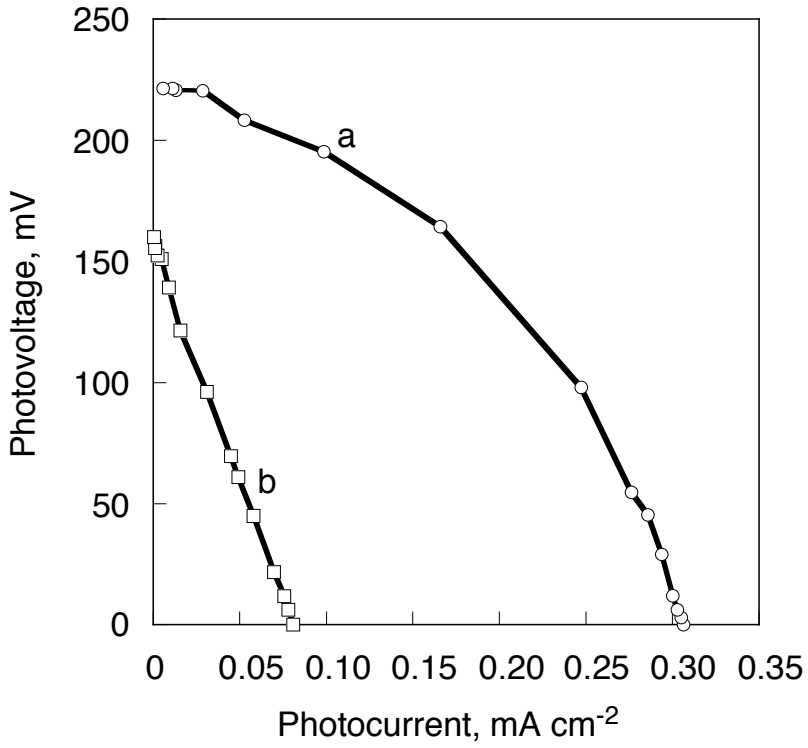


**Fig. 7** Power characteristic of the photoelectrochemical cell under white light ($\lambda > 400$ nm) illumination. Electrodes: (a) OTE/$SnO_2$/(MEH-PPV+$C_{60}$)$_n$, (b) OTE/$SnO_2$/($H_2P$+$C_{60}$)$_n$ and Pt counter electrode, Electrolyte: 0.5 M NaI and 0.01M $I_2$ in acetonitrile, Input power: 11.2 mW/cm$^2$.

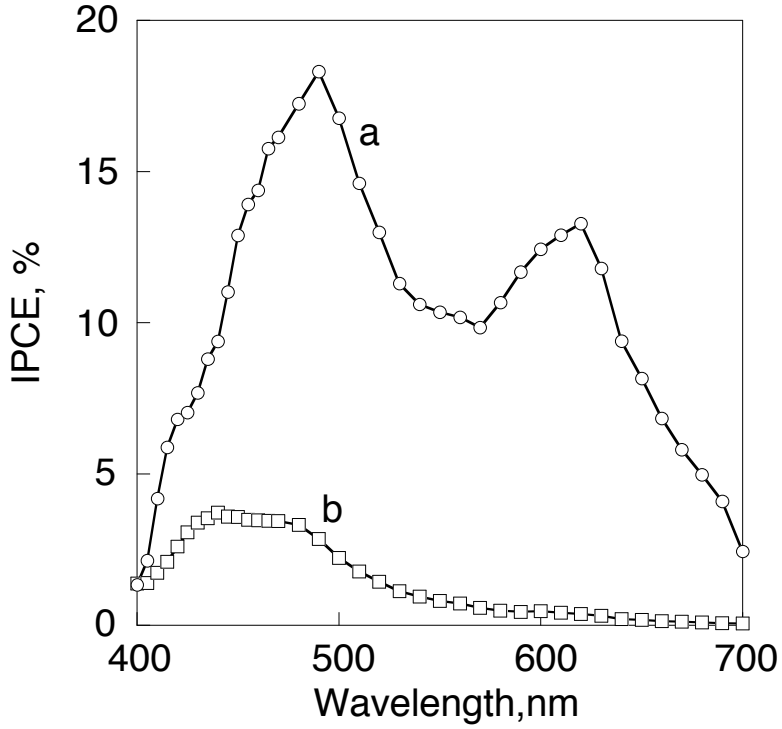


**Fig. 8** The photocurrent action spectra (presented in terms of % IPCE) of (a) OTE/$SnO_2$/(MEH-PPV+$C_{60}$)$_n$ electrode and (b) OTE/$SnO_2$/($H_2$P+$C_{60}$)$_n$ electrode. Electrolyte: 0.5 M NaI and 0.01M $I_2$ in acetonitrile.

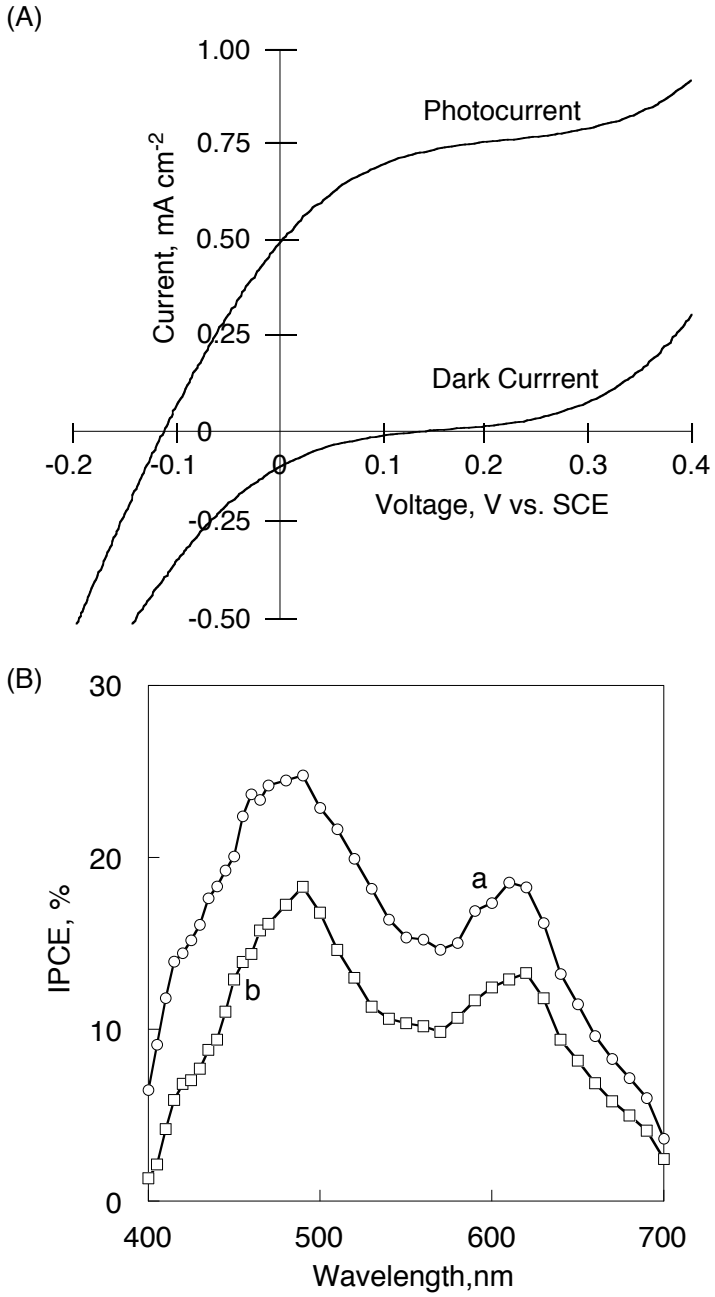


**Fig. 9** (A) *I-V* characteristics of OTE/$SnO_2$/(MEH-PPV+$C_{60}$)$_n$ electrode using saturated calomel reference electrode (SCE) under white light ($\lambda >$ 400 nm) illumination; electrolyte: 0.5 M NaI and 0.01M $I_2$ in acetonitrile, input power: 11.2 mW/cm$^2$. (B) The photocurrent action spectra of (a) OTE/$SnO_2$/(MEH-PPV+$C_{60}$)$_n$ electrode (a) at an applied bias of 0.2 V vs. SCE and (b) with no applied bias potential. Electrolyte: 0.5 M NaI and 0.01M $I_2$ in acetonitrile.

**References and Notes**


1) U. Bach, D. Lupo, P. Comte, J. E. Moser, F. Weissortel, J. Salbeck, H. Spreitzer, and M. Gratzel: Nature **395** (1998) 583.
2) F. Padinger, R. S. Rittberger, and N. S. Sariciftci: Adv. Funct. Mater. **13** (2003) 85.
3) M. Granstrom, K. Petritsch, A. C. Arias, A. Lux, M. R. Andersson, and R. H. Friend: Nature **395** (1998) 257.
4) J. J. M. Halls, C. A. Walsh, N. C. Greenham, E. A. Marseglia, R. H. Friend, S. C. Moratti, and A. B. Holmes: Nature **376** (1995) 498.
5) Martijn M. Wienk, Jan M. Kroon, Wiljan J. H. Verhees, Joop Knol, Jan C. Hummelen, Paul A. van Hal, and R. A. J. Janssen: Angew. Chem., Int. Ed. **42** (2003) 3371.
6) B. O'Regan and M. Gratzel: Nature **353** (1991) 737.
7) S. E. Shaheen, C. J. Brabec, N. S. Sariciftci, F. Padinger, T. Fromherz, and J. C. Hummelen: Appl. Phys. Lett. **76** (2001) 841.
8) W. Ma, C. Yang, X. Gong, K. Lee, and A. J. Heeger: Adv. Funct. Mater. **15** (2005) 1617.
9) P. V. Kamat: J. Phys. Chem. C **111** (2007) 2834.
10) Y. Kim, S. Cook, S. M. Tuladhar, S. A. Choulis, J. Nelson, J. R. Durrant, D. D. C. Bradley, M. Giles, I. McCulloch, C.-S. Ha, and M. Ree: Nature Mater. **5** (2006) 197.
11) G. Li, V. Shrotriya, J. Huang, Y. Yao, T. Moriarty, K. Emery, and Y. Yang: Nature Mater. **4** (2005) 864.
12) I. Gur, N. A. Fromer, M. L. Geier, and A. P. Alivisatos: Science **310** (2005) 462.
13) in *The Photosynthetic Reaction Center* ed. J. Deisenhofer and J. R. Norris (Academic Press, San Diego, 1993).
14) in *Anoxygenic Photosynthetic Bacteria* ed. R. E. Blankenship, M. T. Madigan, and C. E. Bauer (Kluwer Academic Publishing, Dordrecht, 1995).
15) X. Yang, J. Loos, S. C. Veenstra, W. J. H. Verhees, M. M. Wienk, J. M. Kroon, M. A. J. Michels, and R. A. J. Janssen: Nano Lett. **5** (2005) 579.
16) H. Imahori, M. E. El-Khouly, M. Fujitsuka, O. Ito, Y. Sakata, and S. Fukuzumi: J. Phys. Chem. A **105** (2001) 325.
17) H. Imahori, N. V. Tkachenko, V. Vehmanen, K. Tamaki, H. Lemmetyinen, Y. Sakata, and S. Fukuzumi: J. Phys. Chem. A **105** (2001) 1750.
18) S. Fukuzumi and D. M. Guldi: in *Electron Transfer in Chemistry*, ed. V. Balzani (Wiley-VCH, Weinheim, Germany, 2001), Vol. 2, p. 270.
19) S. Fukuzumi: Bull. Chem. Soc. Jpn. **79** (2006) 177.
20) S. Fukuzumi: Pure Appl. Chem. **75** (2003) 577.
21) H. Yamamoto, J. Wilkinson, J. P. Long, K. Bussman, J. A. Christodoulides, and Z. H. Kafafi: Nano Lett. **5** (2005) 2485.
22) D. Braun and A. J. Heeger: Appl. Phys. Lett. **58** (1991) 1982.
23) G. Yu, C. Zhang, and A. J. Heeger: Appl. Phys. Lett. **64** (1994) 1540.
24) G. Yu, K. Pakbaz, and A. J. Heeger: Appl. Phys. Lett. **64** (1994) 3422.

25) M. M. Alam and S. A. Jenekhe: Chem. Mater. **16** (2004) 4647.

26) C. R. McNeill, H. Frohne, J. L. Holdsworth, J. E. Furst, B. V. King, and P. C. Dastoor: Nano Lett. **4** (2004) 219.

27) P. D. Harvey: in *The Porphyrin Handbook*, ed. K. M. Kadish, K. M. Smith, and R. Guilard (San Diego, CA, Academic Press, 2003), Vol. 18, p. 63.

28) F. Diederich and M. Gomez-Lopez: Chem. Soc. Rev. **28** (1999) 263.

29) P. D. W. Boyd and C. A. Reed: Acc. Chem. Res. **38** (2005) 235.

30) D. Sun, F. S. Tham, C. A. Reed, L. Chaker, and P. D. W. Boyd: J. Am. Chem. Soc. **124** (2002) 6604.

31) D. Sun, F. S. Tham, C. A. Reed, and P. D. W. Boyd: PNAS **99** (2002) 5088.

32) J.-Y. Zheng, K. Tashiro, Y. Hirabayashi, K. Kinbara, K. Saigo, T. Aida, S. Sakamoto, and K. Yamaguchi: Angew. Chem., Int. Ed. **40** (2001) 1857.

33) M. M. Olmstead, D. A. Costa, K. Maitra, B. C. Noll, S. L. Phillips, P. M. Van Calcar, and A. L. Balch: J. Am. Chem. Soc. **121** (1999) 7090.

34) Y. B. Wang and Z. Lin: J. Am. Chem. Soc. **125** (2003) 6072.

35) T. Hasobe, H. Imahori, P. V. Kamat, T. K. Ahn, S. K. Kim, D. Kim, A. Fujimoto, T. Hirakawa, and S. Fukuzumi: J. Am. Chem. Soc. **127** (2005) 1216.

36) T. Hasobe, P. V. Kamat, V. Troiani, N. Solladie, T. K. Ahn, S. K. Kim, D. Kim, A. Kongkanand, S. Kuwabata, and S. Fukuzumi: J. Phys. Chem. B **109** (2005) 19.

37) I. Bedja, S. Hotchandani, and P. V. Kamat: J. Phys. Chem. **98** (1994) 4133.

38) T. Hasobe, H. Imahori, S. Fukuzumi, and P. V. Kamat: J. Phys. Chem. B **107** (2003) 12105

39) T. Hasobe, H. Imahori, S. Fukuzumi, and P. V. Kamat: J. Mater. Chem. **13** (2003) 2515.

40) U. Siggel, U. Bindig, C. Endish, T. Komatsu, E. Tsuchida, J. Voigt, and J.-H. Fuhrhop: Ber. Bunsen-Ges. Phys. Chem. **12** (1996) 2070.

41) N. Ballav: Mater. Lett. **59** (2005) 3419.

42) T. Hasobe, S. Fukuzumi, S. Hattori, and P. V. Kamat: Chem. Asian J. **2** (2007) 265.

43) N. V. Tkachenko, H. Lemmetyinen, J. Sonoda, K. Ohkubo, T. Sato, H. Imahori, and S. Fukuzumi: J. Phys. Chem. A **107** (2003) 8834.

44) P. V. Kamat, S. Barazzouk, and S. Hotchandani: Adv. Mater. **13** (2001) 1614.

45) P. V. Kamat, S. Barazzouk, K. George Thomas, and S. Hotchandani: J. Phys. Chem. B **104** (2000) 4014.

46) The broadness of absorption property of OTE/$SnO_2$/(MEH-PPV+$C_{60}$)$_n$ in long wavelength region relative to that in acetonitrile/toluene (3/1, v/v) is due to scattering effects.

47) In photoelectrochemical measurement of OTE/$SnO_2$/(MEH-PPV+$C_{60}$)$_n$, thin film is excited from the backside of an active layer of (MEH-PPV+$C_{60}$)$_n$ as shown in Fig. 5. The difference between photocurrent action and absorption spectra of OTE/$SnO_2$/(MEH-PPV+$C_{60}$) is likely ascribed to the complementary behavior between absorption of $SnO_2$ colloids (short wavelength) and scattering effects (long wavelength).

48) T. Hasobe, H. Imahori, S. Fukuzumi, and P. V. Kamat: J. Phys. Chem. B **107** (2003) 12105.

[49] L. Smilowitz, N. S. Sariciftci, R. Wu, C. Gettinger, A. J. Heeger, and F. Wudl: Phys. Rev. B **47** (1993) 13835.
[50] N. S. Sariciftci, L. Smilowitz, A. J. Heeger, and F. Wudl: Science **258** (1992) 1474.
[51] J. H. Kim and H. Lee: Chem. Mater. **14** (2002) 2270.